scientific reports

OPEN

Relationship and prognostic value of the triglyceride-glucose index and optical coherence tomography-derived physiological index in patients with acute coronary syndrome

Li Pan[1,3], Shiwan Lu[1,3], Qianhang Xia[2,3], Yi Deng[1], Junlin Wu[1], Shitao Luo[1], Chancui Deng[1], Ning Gu[1], Shuangya Yang[1], Guangtao Zhou[1], Xiaoling Fu[1], Ranzun Zhao[1✉], Zhenglong Wang[2✉], Yongchao Zhao[1✉] & Bei Shi[1✉]

The optical flow ratio (OFR), derived from optical coherence tomography (OCT) images, serves as a physiological index, while the Triglyceride-Glucose Index (TyG) is an alternative measure of insulin resistance. Both indices are positively correlated with poor prognosis in patients with acute coronary syndrome (ACS), but the relationship between the TyG index, OFR, and their prognostic value remains unclear. We included ACS patients who underwent OCT between January 1, 2021, and March 31, 2023. The TyG index was calculated as Ln[fasting triglycerides (mg/dL) × fasting blood glucose (mg/dL)/2]. Patients were grouped into three categories (T1, T2, and T3) based on TyG tertiles. The primary endpoint was major adverse cardiovascular events (MACE). In our analysis, the T3 group showed a significantly higher incidence of MACE ($P < 0.05$), with a progressive decrease in vessel-level OFR observed as the TyG index increased, demonstrating a linear correlation ($r = -0.0146$, $P < 0.001$). The restricted cubic splines (RCS) model revealed a nonlinear relationship between the TyG index and the likelihood of MACE (P for nonlinear < 0.021). Additionally, the cumulative incidence of MACE was significantly higher in patients with a higher TyG index (all Log-rank $P < 0.001$).These findings suggest a nonlinear relationship between the TyG index and MACE, and a linear association between the TyG index and vessel-level OFR. The combination of the TyG index and OFR significantly improved discriminatory ability (c-index: 0.720 vs. 0.757; $P < 0.001$) and reclassification ability (net reclassification index [NRI]: 0.373; integrated discrimination improvement [IDI]: 0.031; $P < 0.0001$) for predicting MACE compared to vessel-level OFR alone. This combination effectively identifies high-risk ACS patients.

Keywords Acute coronary syndrome, Insulin resistance, Optical coherence tomography, Intracoronary imaging, Computed physiology

Abbreviations

ACS	Acute coronary syndrome
AMI	Acute myocardial infarction
AUC	Area under the curve
BMI	Body mass index
CAD	Coronary artery disease
CCB	Calcium channel blockers

[1]Department of Cardiology, Affiliated Hospital of Zunyi Medical University, Zunyi 563000, China. [2]Department of Cardiology, The Third Affiliated Hospital of Zunyi Medical University, No. 98 Fenghuang North Road, Xima Road Street, Huichuan District, Zunyi 563000, China. [3]Li Pan, Shiwan Lu and Qianhang Xia contributed equally to this work. ✉email: kouke80@126.com; wangzhenglong321@163.com; yongchaozhao@zmu.edu.cn; shib@zmu.edu.cn

CI	Confidence interval
CVE	Cardiovascular events
DALYs	Disability-adjusted life years
DES	Drug eluting stent
eGFR	Estimated glomerular filtration rate
FFR	Fractional flow reserve
HDL-C	High-density lipoprotein cholesterol
HOMA-IR	Homeostasis model assessment of insulin resistance
IEL	Internal elastic lamina
IR	Insulin resistance
ISR	in-stent restenosis
LAD	Left anterior descending
LCR	Lipid-to-cap ratio
LCX	Left circumflex artery
LDL-C	Low-density lipoprotein cholesterol
MACE	Major adverse cardiovascular events
MLA	Minimum lumen area
NCL	Non-culprit lesion
NRI	Net reclassification index
NTproBNP	N-Terminal pro-B-type natriuretic peptide
OCT	Optical coherence tomography
OFR	Optical flow ratio
OGTT	Oral glucose tolerance test
PCI	Percutaneous coronary intervention
POCO	Patient-oriented composite outcome
RCA	Right coronary artery
RCS	Restricted cubic spline
ROC	Receiver operating characteristic curve
STEMI	ST-elevation myocardial infarction
TBIL	Total bilirubin
TC	Total cholesterol
TG	Triglyceride
TLR	Target lesion revascularization
TVF	Target vessel failure
TyG	Triglyceride-glucose
T2DM	Type 2 diabetes
UA	Unstable angina

Coronary artery disease (CAD) is a leading cause of death globally and a major contributor to the loss of disability-adjusted life years (DALYs)[1]. Despite the widespread use of secondary prevention therapies and revascularization techniques, patients with CAD remain at high risk for recurrent ischemic cardiovascular events, particularly those with acute coronary syndrome (ACS)[2,3]. Therefore, early identification of high-risk patients is essential for improving risk stratification and optimizing treatment management.

Insulin resistance (IR), characterized by reduced insulin sensitivity and often preceding type 2 diabetes mellitus (T2DM), is commonly assessed using the Homeostasis Model Assessment of Insulin Resistance (HOMA-IR). However, its utility is limited in individuals on insulin therapy or with dysfunctional β-cells[4,5]. The Triglyceride-Glucose (TyG) index, developed as a simple, convenient, and cost-effective alternative, has been shown to outperform HOMA-IR in assessing IR[6]. The TyG index is a reliable and accessible biomarker for evaluating IR in patients with coronary artery disease (CAD)[7,8]. Recent studies indicate that the TyG index is associated with disease progression, prognosis, and risk stratification in patients with CAD and acute coronary syndrome (ACS)[9–12].

Optical coherence tomography (OCT) is an intracoronary imaging technique that employs infrared light emission to obtain detailed in vivo images of coronary artery plaques. By measuring the echo time delay and intensity of light reflected or scattered from the internal structure of tissue, OCT provides high-resolution morphological characterization of plaques[13,14]. Zhao et al. investigated the relationship between the TyG index and cardiovascular outcomes in patients with acute ST-segment elevation myocardial infarction (STEMI), focusing particularly on its association with plaque morphology. Their study concluded that the TyG index, when combined with plaque morphological characteristics, can help stratify risk in STEMI patients and predict adverse events[15]. Recent advancements in deep learning-based artificial intelligence algorithms have facilitated the calculation of OCT-derived coronary computed physiology and plaque morphology. These algorithms have demonstrated strong diagnostic performance in prior studies. The optical flow ratio (OFR), a computed physiological function derived from OCT, has been shown to correlate well with wire-based fractional flow reserve (FFR)[16–22].

Previous studies have elucidated potential mechanistic links between insulin resistance, coronary physiology, and early prognosis. Otsuka et al. employed coronary computed tomography angiography (CCTA) to evaluate coronary plaque burden. Their study identified both diabetes mellitus (DM) and the TyG index as predictors of poor prognosis in patients with chronic coronary syndrome (CCS), independent of coronary plaque volume. DM patients exhibited the highest plaque burden and coronary artery calcium (CAC) scores among the three groups, reinforcing the association between an elevated TyG index and increased coronary atherosclerotic burden and

early prognosis[23]. Nakanishi et al. investigated the predictive value of coronary flow reserve (CFR) for long-term cardiovascular prognosis in patients with chronic kidney disease (CKD). Their findings indicated that C-reactive protein levels and CFR values were independent predictors of cardiovascular events, irrespective of traditional cardiovascular risk factors. The coronary physiological index CFR may aid in stratifying cardiovascular risk and predicting adverse outcomes in CKD patients[24].

This study explores the combined predictive value of the TyG index and immediate post-procedural OFR in forecasting adverse outcomes in patients with ACS. It demonstrates the correlation and predictive power of the TyG index and post-procedural OFR in this patient population.

Methods

Study population and definitions

Patients diagnosed with ACS and admitted to the cardiology department of the Affiliated Hospital of Zunyi Medical University between January 1, 2021, and December 31, 2023, were included in this study. The inclusion criteria were: (1) age between 18 and 80 years; (2) completion of OCT examination following the procedure; and (3) provision of signed informed consent. The exclusion criteria included: (1) poor or missing OCT image quality post-procedure; (2) in-stent restenosis (ISR); (3) left main coronary lesions; (4) chronic total occlusion; and (5) patients lost to follow-up. A total of 1,056 ACS patients were ultimately enrolled and categorized into three groups based on TyG index tertiles (Fig. 1).

ACS, including unstable angina (UA) and acute myocardial infarction (AMI), was diagnosed according to the fourth universal definition of myocardial infarction (MI)[25]. Diabetes was diagnosed if any of the following criteria were met: (1) HbA1c $\geq$ 6.5%; (2) random blood glucose $\geq$ 11.1 mmol/L; (3) fasting blood glucose $\geq$ 7.0 mmol/L; or (4) 2-hour venous plasma glucose $\geq$ 11.1 mmol/L during an oral glucose tolerance test (OGTT). Hypertension was defined as a systolic blood pressure $\geq$ 140 mmHg or diastolic blood pressure $\geq$ 90 mmHg, either at rest or during antihypertensive treatment. Body mass index (BMI) was calculated using the formula: BMI (kg//m^2) = body weight (kg) / height^2 (m^2). This retrospective study was conducted in accordance with the principles of the Declaration of Helsinki. Ethical review procedures, including patient consent, were approved by the Biomedical Research Ethics Committee of the Affiliated Hospital of Zunyi Medical University, following the guidelines of the National Health and Safety Commission of China. Given the retrospective nature of the study, the institutional review board waived the requirement for informed consent and the disclosure of patient identity information.

OCT image analysis and definition

The PCI procedures were performed in the catheterization laboratory of the Department of Cardiology at the Affiliated Hospital of Zunyi Medical University. At the conclusion of the procedure, OCT imaging was performed with a frequency-domain OCT system (ILUMIEN; Abbott Vascular), coupled with a Dragonfly™ Optis™ OCT imaging catheter (Abbott Vascular). An image of the entire length of the culprit blood vessel was obtained using a pullback device that moved automatically at a speed of 36 mm/s, and cross-sectional images were generated at a rotation rate of 180 frames/s. The analysis was performed by two independent intravascular imaging technicians, blinded to the clinical outcomes of the patients. In patients with multivessel disease, the culprit vessel was defined as the vessel with the most severe stenosis (> 70%) or the coronary artery with the most significant ischemia or infarction on the electrocardiogram. The target vessel was divided into three longitudinal subsegments: (1) the stent segment, (2) an adjacent reference segment ($\leq$ 5 mm in length), and (3) the non-culprit lesion segment (NCL). NCL refers to an untreated coronary artery segment with a diameter stenosis greater than 30% on angiography, located at least 5 mm away from the stent. If multiple NCLs were present, the segment with the most severe stenosis was selected for analysis[22]. In this study, Anonymous OCT images were analyzed by experienced analysts using dedicated quantitative analysis software (OctPlus, version 2.0, Pulse Medical Imaging Technology, Shanghai, China). All OCT image frames were meticulously analyzed to assess plaque composition, including lipid-rich, fibrous, and calcified components. The software also enabled automatic delineation of the internal elastic lamina (IEL) and quantified the plaque burden associated with each constituent subtype of atherosclerotic lesions. PB was calculated as the area between the estimated IEL contour and the lumen contour, divided by the IEL area, and multiplied by 100%[16]. The LCR was automatically calculated based on an AI model that accounts for both the lipid burden of the plaque and the cap thickness of the NCL area. The maximum LCR was measured from an OCT frame of the NCL in the culprit vessel. If multiple NCLs were present in the culprit vessel, the maximum LCR was defined as the highest LCR among them and was used for analysis at the culprit vessel level[21].

Evaluation of OCT-derived coronary physiology function

Previous studies have demonstrated that AI algorithms can be employed to determine the internal diameter of a pipe while adhering to the law of conservation of mass (the incompressibility of fluids). By adjusting parameters to simulate the pressure-reducing effect at different pressures and temperatures, the OFR can be derived. Quantitative analysis software (OctPlus, version 2.0, Pulse Medical Imaging Technology, Shanghai, China). was used to calculate the OFR from OCT cross-sectional areas, following the algorithm described previously[26]. This algorithm is based on the following equation, which incorporates fluid dynamics:

$$\Delta P = FV + SV^2$$

where V is the flow velocity, F is the pressure loss coefficient due to viscous friction (Poiseuille resistance), and S is the local pressure loss coefficient due to sudden amplification (blood flow separation)[22]. We evaluated the
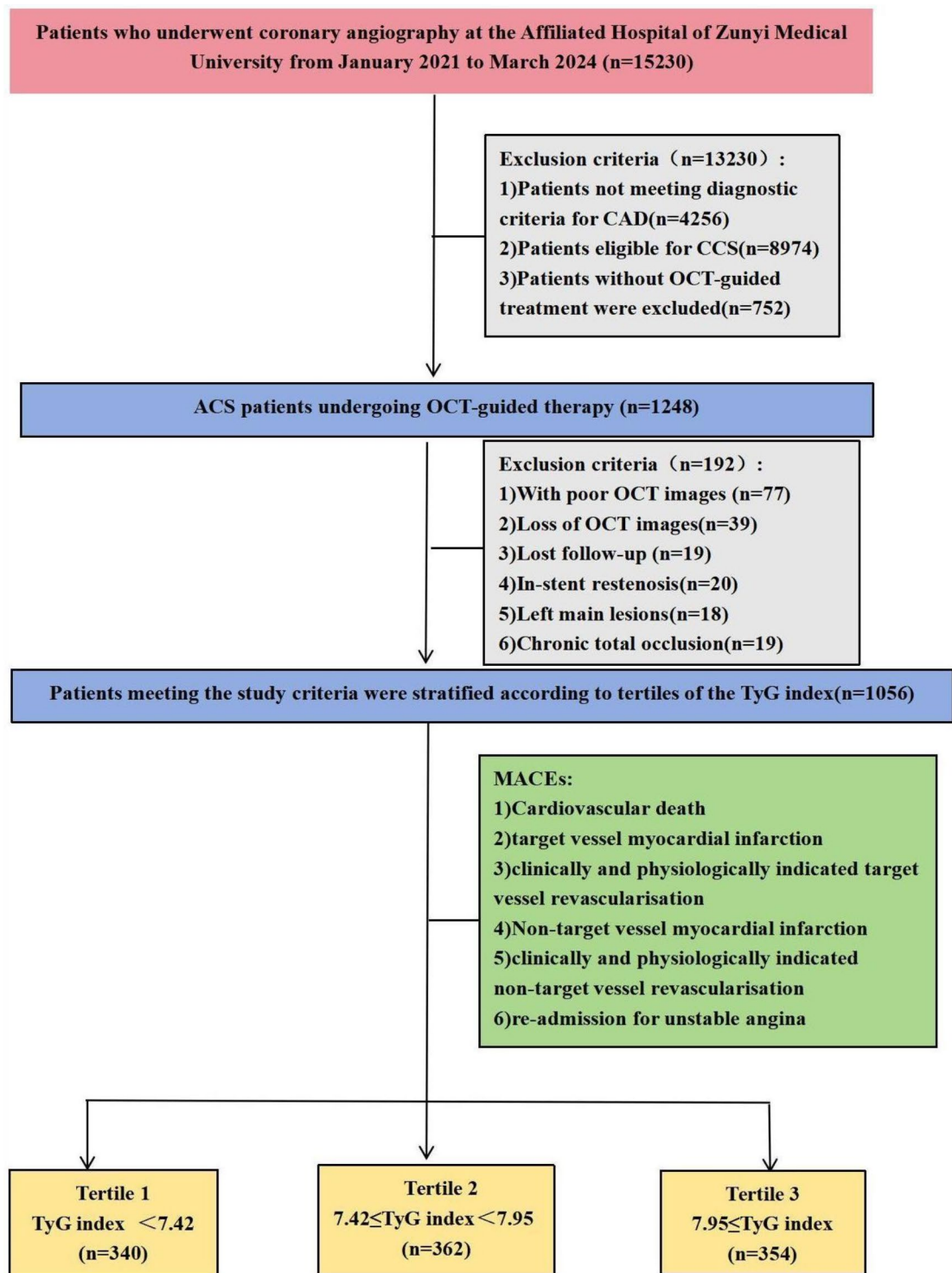
Fig. 1. Flow diagram of patient selection. *TyG* triglyceride-glucose, *MACE* major adverse cardiovascular event, *CAD* coronary artery disease, *ACS* acute coronary syndrome, *CCS* chronic coronary syndrome, *OCT* optical coherence tomography;

plaque morphological characteristics of the NCL and the vessel-level OFR of the culprit vessel in ACS patients after PCI. A typical case of post-procedural OCT image analysis using AI software is shown in Fig. 2.

Feature selection

The Boruta algorithm is an extension of the Random Forest method, designed for feature selection. It operates by creating "shadow features," which are random recombinations of the original features. This technique is particularly useful for identifying critical features associated with outcomes such as MACE risk or for generating radiomics features. The Boruta algorithm works by generating copies of the real features, known as shadow features, and comparing the importance of these features based on their z-scores. In each iteration, a Random Forest classifier is used to assess the importance of both the real and shadow features. The z-scores of each feature are computed based on their contribution to the model. The highest z-score among the shadow features is recorded. If the z-score of a real feature exceeds this maximum, the feature is deemed important and confirmed. Conversely, if the real feature's z-score is lower than that of the shadow features, it is rejected; otherwise, it remains tentative.

Follow-up and endpoints

Follow-up and endpoint assessment were conducted by trained clinicians, either in outpatient clinics or via telephone, with a median follow-up duration of 687 days (IQR: 494–852 days). Follow-up was discontinued upon the occurrence of endpoints or on 1 October 2024. Data were recorded on a standardized computerized case report form. Endpoint events were adjudicated independently by three cardiovascular experts, who were blinded to patient information. In cases of disagreement, a consensus decision was reached through discussion. The primary
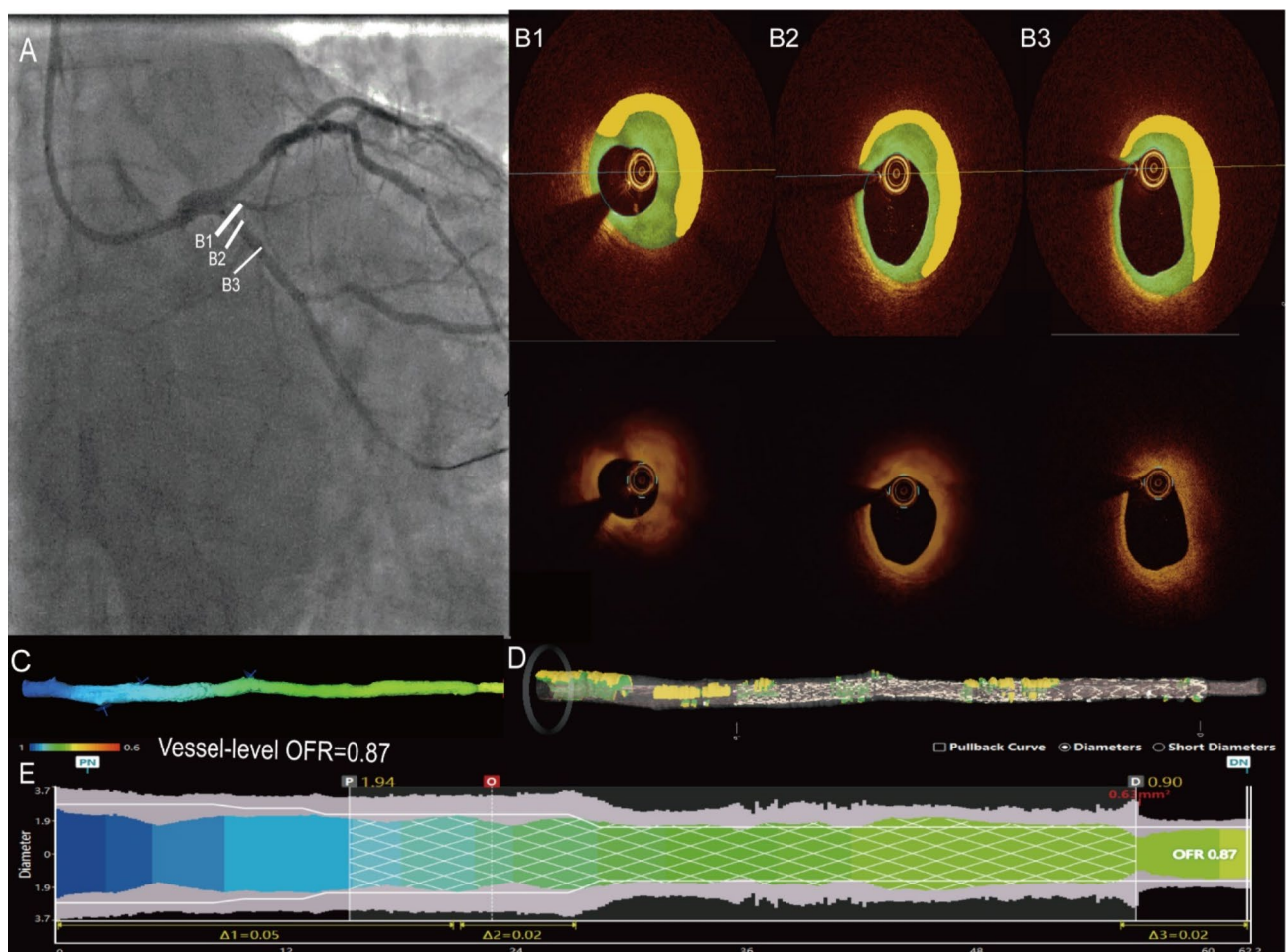

Fig. 2. Typical examples of non-culprit lesions identified through deep learning algorithms for the simultaneous detection of both morphological and physiological characteristics. (**A**) Coronary angiography shows a moderate lesion in the proximal segment of the left circumflex artery, identified as a non-culprit lesion. (**B**) OCT reveals lipid and fibrous plaques (**B1–B3**). (**C**) The calculated OFR measurements are depicted using a color-coded method. (**D**) Three-dimensional reconstruction of the lumen, with overlaying plaque composition. (**E**) OFR values are color-coded and displayed on the lumen diameter distribution plot. The most distal OFR value is 0.87. *CAG* coronary angiography, *LCx* left circumflex artery, *OCT* optical coherence tomography, *OFR* optical flow ratio;

endpoint of this trial was defined as the composite of the first occurrence of MACE during follow-up. MACE was defined as follows: (1) Cardiac death; (2) Unplanned revascularization, defined as repeat revascularization for unexpected cardiac reasons, including unplanned target and non-target vessel revascularization; (3) Non-fatal myocardial infarction, defined as myocardial necrosis without death, accompanied by symptoms of ischemia, abnormal cardiac markers, ST-segment changes, or pathological Q-wave changes (including both target and non-target vessel); and (4) Re-admission for unstable angina.

Statistical analysis

For normal distributions, continuous variables are expressed as mean ± standard deviation (SD), and for skewed distributions, continuous variables are expressed as median (IQR). Categorical variables are expressed as numbers (percentage). The t-test or ANOVA is used for intergroup comparisons of continuous variables if they are normally distributed, and the Mann-Whitney u test or Kruskal-Wallis test is used if they are not normally distributed. Categorical variables were compared using Pearson's chi-squared (X^2) test or Fisher's exact test as the case may be.

A boruta-based feature selection method was used to identify potential features associated with the endpoint. The cumulative incidence of terminal events was described using the Kaplan-Meier method, and the log-rank test was used to obtain the P value for comparisons between groups. The association between the TyG index and the endpoint was examined using a multivariate Cox proportional hazards model, and the results are expressed as hazard ratio (HR) and 95% confidence interval (CI). Risk factors that were statistically significant ($P < 0.05$) in univariate analysis and selected by the Boruta algorithm, among which the TyG index and vessel-level OFR were both statistically significant. In addition to the crude model, which did not adjust for confounders, three other models were fitted. Pearson or Spearman correlation analysis was used to determine the correlation between the TyG index and vessel OFR. In addition, multivariate restricted cubic spline (RCS) analysis was used to assess any potential non-linear relationship between the TyG index and the endpoint. The area under the receiver operating characteristic (ROC) curves was used to indicate the predictive value of the TyG index and vessel-level OFR for MACE. To assess whether the addition of vascular OFR to the TyG index has incremental predictive value for MACE, we compared the C-index, net reclassification improvement (NRI) and integrated discrimination improvement (IDI) between the models. We conducted subgroup analyses to assess whether the combined predictive value of the TyG index and vessel-level OFR for MACE varied across different subgroups. The sample was divided into high-risk and low-risk groups based on the risk score derived from a Cox proportional hazards model, and the interaction p-value was calculated. A two-sided analysis with a P value < 0.05 was considered significant. All analyses were performed using SPSS 29.0 (IBM Corp, Armonk, NY, USA, version 29.0) and R version 4.2.3 (R Foundation for Statistical Computing, Vienna, Austria).

Results

Baseline characteristics

Baseline clinical characteristics and clinical events were fully recorded for 1056 patients. The median age of patients was 59 years [IQR: 52–70 years], and 881 cases (83.4%) were male. All participants were stratified into three groups: T1 (TyG index < 7.42, $n = 340$), T2 ($7.42 \leq$ TyG index < 7.95, $n = 362$), and T3 (TyG index ≥ 7.95, $n = 354$) in accordance with the TyG index tertiles. ACS patients with a high TyG index (T3 group) are more prone to diabetes, dyslipidemia, and MACE. They also exhibit higher BMI, FBG, triglycerides, total cholesterol, low-density lipoprotein cholesterol, and apolipoprotein B, as well as lower high-density lipoprotein cholesterol. Notably, the rate of metformin use in the T1 group (5.29%) was significantly lower than in the T2 (12.15%) and T3 (13.56%) groups ($P < 0.001$), and there were no significant differences in other baseline characteristics (Table 1).

Angiography and OCT quantitative morphofunctional characteristics

Table 2 presents a comparison of angiographic and OCT-derived morphofunctional characteristics, stratified by quantiles of the TyG index. Angiographic characteristics, including the location of the culprit vessel and whether the lesion was distal, differed significantly among the three groups ($P < 0.05$). Post-procedural OCT results showed that both the proximal and distal reference diameters were lowest in the T3 group, with statistically significant differences between the groups ($P < 0.05$). The relative MLA and average lumen area in the T3 group were significantly lower than those in the T1 and T2 groups ($P < 0.01$), while the average reference area was also the lowest in the T3 group ($P < 0.05$). No significant differences were observed in stent-related characteristics among the three groups. The PB, LCR, and maximum lipid area in the T3 group were higher than those in the other two groups ($P < 0.05$). Among the morphological characteristics identified by artificial intelligence, macrophage volume was greatest in the T3 group, with a statistically significant difference ($P = 0.048$). Additionally, post-procedural vessel-level OFR, lesion residual OFR, and stent residual OFR in the T3 group were lower than those in the other two groups ($P < 0.05$).

Feature selection results

A total of 82 variables were included in the analysis. Following 100 iterations of the Boruta feature selection method, 16 features with the highest correlation to MACE risk were identified, including the TyG index and vessel-level OFR. The status of the remaining 4 features remains tentative (Fig. 3). When the z-scores of the TyG index and vessel-level OFR exceed those of the shaded features in the Boruta analysis, they demonstrate the largest matched effect among a set of biomarkers (maximum, mean, and minimum), indicating their predictive value for MACE.

Variables	Total ($n=1056$)	T1 ($n=340$)	T2 ($n=362$)	T3 ($n=354$)	P value
TyG index	7.66 (7.31, 8.18)	7.18 (7.07, 7.29)	7.65 (7.53, 7.79)	8.45 (8.18, 8.92)	**<0.001**
MACEs (n, %)	133 (12.59)	20 (5.88)	33 (9.12)	80 (22.60)	**<0.001**
Demographics					
Age (years)	59.00 (52.00, 70.00)	60.00 (51.75, 70.25)	60.00 (53.00, 70.00)	58.00 (52.00, 69.00)	0.376
Male (n, %)	881 (83.43)	288 (84.71)	300 (82.87)	293 (82.77)	0.743
BMI (kg/m^2)	24.17 (22.15, 26.31)	23.48 (22.04, 25.71)	24.16 (21.97, 26.33)	24.61 (22.79, 26.92)	**<0.001**
Heart rate (bpm)	76.00 (69.00, 85.00)	76.00 (68.00, 83.25)	76.00 (69.00, 85.00)	76.00 (68.25, 86.00)	0.534
SBP (mmHg)	127 (113, 140)	126 (113, 140)	127 (116, 140)	128 (112, 140)	0.595
DBP (mmHg)	79.00 (70.00, 88.00)	78.00 (70.00, 87.00)	80.00 (72.00, 89.00)	78.50 (69.00, 88.00)	0.255
Comorbidity					
Hypertension (n, %)	584 (55.30)	183 (53.82)	198 (54.70)	203 (57.34)	0.621
Diabetes mellitus (n, %)	220 (20.83)	38 (11.18)	82 (22.65)	100 (28.25)	**<0.001**
Dyslipidemia (n, %)	233 (22.06)	36 (10.59)	76 (20.99)	121 (34.18)	**<0.001**
Smoking history (n, %)	542 (51.33)	187 (55.00)	174 (48.07)	181 (51.13)	0.184
Chronic heart failure (n, %)	44 (4.17)	13 (3.82)	11 (3.04)	20 (5.65)	0.202
Stroke (n, %)	54 (5.11)	16 (4.71)	22 (6.08)	16 (4.52)	0.587
Chronic kidney disease (n, %)	32 (3.03)	7 (2.06)	10 (2.76)	15 (4.24)	0.230
Diagnosis on admission					
STEMI (n, %)	429 (40.62)	150 (44.12)	138 (38.12)	141 (39.83)	0.253
NSTEMI (n, %)	235 (22.25)	72 (21.18)	86 (23.76)	77 (21.75)	0.686
UA (n, %)	390 (36.93)	120 (35.29)	137 (37.85)	133 (37.57)	0.747
Discharge therapy					
Aspirin/Indobufen (n, %)	995 (94.22)	318 (93.53)	342 (94.48)	335 (94.63)	0.798
Clopidogrel/Ticagrelor (n, %)	991 (93.84)	320 (94.12)	340 (93.92)	331 (93.50)	0.942
Statin (n, %)	876 (82.95)	273 (80.29)	309 (85.36)	294 (83.05)	0.203
Beta-blockers (n, %)	811 (76.80)	252 (74.12)	275 (75.97)	284 (80.23)	0.146
ACEI/ARB/ARNI (n, %)	672 (63.64)	221 (65.00)	227 (62.71)	224 (63.28)	0.807
Ezetimibe Tablets (n, %)	122 (11.55)	37 (10.88)	43 (11.88)	42 (11.86)	0.895
CCB (n, %)	99 (9.38)	32 (9.41)	29 (8.01)	38 (10.73)	0.458
SGLT2 (n, %)	131 (12.41)	40 (11.76)	47 (12.98)	44 (12.43)	0.887
Metformin (n, %)	110 (10.42)	18 (5.29)	44 (12.15)	48 (13.56)	**<0.001**
Nicorandil (n, %)	425 (40.25)	132 (38.82)	152 (41.99)	141 (39.83)	0.681
PCSK9 (n, %)	183 (17.33)	63 (18.53)	55 (15.19)	65 (18.36)	0.415
Insulin (n, %)	51 (4.83)	10 (2.94)	20 (5.52)	21 (5.93)	0.138
Laboratory results					
FBG (mmol/L)	6.58 (5.36, 8.65)	5.49 (4.84, 6.41)	6.79 (5.59, 8.40)	8.29 (6.39, 12.69)	**<0.001**
Triglycerides (mmol/L)	1.91 (1.47, 2.92)	1.46 (1.25, 1.67)	1.90 (1.57, 2.34)	3.47 (2.59, 5.25)	**<0.001**
Total cholesterol (mmol/L)	4.83 (3.98, 5.62)	4.67 (3.89, 5.38)	4.79 (3.99, 5.47)	5.08 (4.10, 5.96)	**<0.001**
HDL-C (mmol/L)	1.10 (0.95, 1.28)	1.16 (1.00, 1.33)	1.10 (0.97, 1.30)	1.07 (0.92, 1.23)	**<0.001**
LDL-C (mmol/L)	2.91 (2.30, 3.48)	2.82 (2.20, 3.36)	2.92 (2.32, 3.41)	3.04 (2.39, 3.60)	**0.015**
Apolipoprotein A1 (mmol/L)	1.20 (1.06, 1.34)	1.20 (1.07, 1.36)	1.19 (1.08, 1.34)	1.21 (1.05, 1.33)	0.540
Apolipoprotein B (mmol/L)	0.92 (0.73, 1.12)	0.89 (0.70, 1.07)	0.93 (0.74, 1.11)	0.96 (0.73, 1.16)	**0.040**
Urea, mmol/L (mmol/L)	5.10 (4.20, 6.30)	5.10 (4.20, 6.50)	5.10 (4.20, 6.29)	5.20 (4.20, 6.20)	0.878
Uric acid (mmol/L)	345.50 (289.00, 410.00)	338.50 (276, 401.25)	348. (293.50, 413.50)	350 (293.25, 410.75)	0.067
Creatinine (µmmol/L)	78.00 (67.00, 92.00)	79.00 (67.00, 94.00)	77.00 (67.00, 91.00)	79.00 (68.00, 92.00)	0.741
Continued					

Variables	Total ($n = 1056$)	T1 ($n = 340$)	T2 ($n = 362$)	T3 ($n = 354$)	P value
eGFR (mL/min/1.73 m^2)	91.48 (68.65, 107.44)	90.88 (65.60, 107.37)	92.65 (69.65, 107.45)	91.80 (69.83, 107.51)	0.627
Fibrinogen (g/L)	3.08 (2.56, 3.85)	3.06 (2.54, 3.85)	3.13 (2.58, 3.84)	3.10 (2.56, 3.87)	0.875
NTProBNP (ng/L)	242.50 (80.00, 888.50)	255.50 (89.75, 926.75)	282 (88.50, 1030.50)	209 (71.25, 729.00)	0.162
Myoglobin (ng/ml)	42.00 (23.00, 172.00)	43.00 (24.00, 172.00)	40.00 (23.00, 175.50)	43.00 (23.00, 167.75)	0.842
Hs-cTn (ng/ml)	78.81 (11.79, 505.05)	86.95 (13.13, 570.12)	81.09 (12.07, 501.35)	62.97 (9.69, 418.57)	0.291

Table 1. Baseline clinical and laboratory characteristics of the study population according to the TyG index tertiles. *TyG* triglyceride-glucose, *T1* tertile 1, *T2* tertile 2, *T3* tertile 3, *MACEs* major adverse cardiovascular events, *BMI* body mass index, *SBP* systolic blood pressure, *DBP* diastolic blood pressure, *STEMI* ST-segment elevation myocardial infarction, *NSTEMI* Non-ST-segment elevation myocardial infarction, *UA* unstable angina, *ACEI* angiotensin converting enzyme inhibitor, *ARB* angiotensin receptor blocker, *ARNI* angiotensin receptor neprilysin inhibitor, *CCB* calcium channel blockers, *SGLT2* sodium-glucose co-transporter 2 inhibitors, *PCSK9* proprotein convertase subtilisin/kexin type 9 inhibitors, *FBG* fasting blood glucose, *HDL-C* high-density lipoprotein cholesterol, *LDL-C* low-density lipoprotein cholesterol, *eGFR* Estimated glomerular filtration rate, *BNP* brain natriuretic peptide, *Hs-cTn* high-sensitivity cardiac troponin. Bold values represent $P < 0.05$.

Association between the TyG index and vessel-level OFR in ACS patients

Figure 4 shows the correlation between the TyG index and vessel-level OFR. The results demonstrate that the TyG index in ACS patients is inversely correlated with vessel-level OFR ($r = -0.146$, $P < 0.001$). This finding suggests that as the TyG index increases, the OFR value decreases. In ACS patients, a reduction in coronary physiological function is more likely to result in vessel-specific ischemia, potentially leading to AMI, and lower level of post-procedure vessel-level OFR also predicted a high risk of MACE after procedure. The ROC curve for vessel-level OFR is shown in Supplementary Fig. S1. Vessel-level OFR was categorized using a cutoff value of 0.90, with a sensitivity of 0.586 and specificity of 0.748.

Comparisons of the TyG index between the low and high OFR groups are shown in Supplementary Fig. S2. The TyG index was significantly higher in the high OFR group compared to the low OFR group ($P = 0.002$). The distribution of vessel-specific ischemia (vessel-level OFR < 0.9) across different TyG level groups is shown in Supplementary Fig S3. Vessel-specific ischemia occurred at a significantly higher rate in the T3 group compared to the other two groups ($P = 0.012$).

Association between the TyG index and endpoints

A multivariate restricted cubic spline (RCS) analysis was performed to explore both linear and nonlinear associations between the TyG index and endpoints in ACS patients after PCI. As shown in Fig. 5, a nonlinear relationship was observed between the TyG index and the probability of MACE according to the RCS model (P for nonlinear < 0.021). Patients were categorized into three groups based on TyG index tertiles. The Kaplan-Meier survival curves for endpoints, stratified by TyG index tertiles, are presented in Fig. 6A. The cumulative incidence of MACE was significantly higher in patients with a higher TyG index compared to those with a lower TyG index (all log-rank $P < 0.001$).

Table 3 summarizes the results of a multivariate Cox proportional hazards regression analysis, which reveals a significant association between a higher TyG index and an increased risk of MACE (HR 2.149, 95% CI 1.762–2.622, $P < 0.001$). The unadjusted model showed a statistically significant association between the TyG index and MACE. In Model 3, after further adjustments for the traditional cardiovascular risk factors, laboratory indicators and OCT-derived morphological index, the TyG index continued to be independently associated with MACE (HR 2.279, 95% CI 1.798–2.889, $P < 0.001$). Using T1 as the reference, the risk of the primary endpoint in the T3 group was 1.760 times higher in the original model (HR 1.760, 95% CI 1.239–2.501, $P = 0.002$), with similarly elevated risks observed in Models 1, 2, and 3. The trend analysis from T1 to T3 across all models was statistically significant (P for trend < 0.001).

Independent and additive prognostic implications of post-procedural vessel-level OFR in ACS patients

Table 3 presents the results of the Cox proportional hazards regression analysis assessing vessel-level OFR as a predictor of MACE. The original model indicated that a lower vessel-level OFR was associated with an increased risk of MACE (HR per 0.1 increase = 0.560, 95% CI 0.481–0.652, $P < 0.001$). Furthermore, vessel-level OFR remained a significant prognostic factor across all three models after adjusting for confounding variables ($P < 0.01$). Kaplan-Meier survival curves for endpoints, stratified by TyG index tertiles combined with different levels of vessel-level OFR, are shown in Fig. 6B. The cumulative incidence of MACE was significantly higher in patients with a higher TyG index and lower postoperative vessel-level OFR than in the other groups (all log-rank $P < 0.001$). Figure 7 illustrates the concordance index (c-index) for predicting MACE using the TyG index, vessel-level OFR, and their combination. Compared to vessel-level OFR alone, the combination of TyG and OCT-derived computational physiology demonstrated significantly improved discriminatory ability (c-index: 0.720 vs. 0.757; $P < 0.001$) and reclassification ability (NRI: 0.373; relative IDI: 0.031; $P < 0.001$) for predicting MACE. In this study, the TyG index, as an independent risk factor, when combined with OCT-derived physiology

Variables	Total (n = 1056)	T1 (n = 340)	T2 (n = 362)	T3 (n = 354)	P value
Pre-procedural angiographic characteristics					
Diameter stenosis rate(%)	90 (80.00, 100.00)	90 (80.00, 99.00)	90 (80.00, 100.00)	90 (80.00, 100.00)	0.829
Coronary lesions (n, %)					0.662
One-vessel disease	445 (42.14)	142 (41.76)	150 (41.44)	153 (43.22)	
Two-vessel disease	306 (28.98)	107 (31.47)	105 (29.01)	94 (26.55)	
Three-vessel disease	305 (28.88)	91 (26.76)	107 (29.56)	107 (30.23)	
Target vessel (n, %)					**0.003**
LAD	505 (47.82)	156 (45.88)	171 (47.24)	178 (50.28)	
LCX	175 (16.57)	39 (11.47)	70 (19.34)	66 (18.64)	
RCA	376 (35.61)	145 (42.65)	121 (33.43)	110 (31.07)	
Lesion segment (n, %)					
Proximal	378 (35.80)	131 (38.53)	126 (34.81)	121 (34.18)	0.436
Middle	541 (51.23)	179 (52.65)	177 (48.90)	185 (52.26)	0.545
Distal	162 (15.34)	40 (11.76)	67 (18.51)	55 (15.54)	**0.046**
Lesion type (n, %)					0.482
Focal lesion	853 (80.78)	278 (81.76)	293 (80.94)	282 (79.66)	
Diffuse lesion	192 (18.18)	58 (17.06)	65 (17.96)	69 (19.49)	
Specific lesion type (n, %)					
Bifurcation lesion	266 (25.19)	86 (25.29)	82 (22.65)	98 (27.68)	0.300
Calcified lesion	89 (8.43)	34 (10.00)	27 (7.46)	28 (7.91)	0.438
Chronic total occlusive lesion	52 (4.92)	21 (6.18)	16 (4.42)	15 (4.24)	0.429
Quantitative variables of post-procedural OCT					
Lesion results					
Proximal reference diameter (mm)	3.75 (3.40, 4.09)	3.80 (3.47, 4.14)	3.76 (3.39, 4.10)	3.67 (3.34, 4.04)	**0.031**
Distal reference diameter (mm)	3.01 (2.62, 3.40)	3.12 (2.65, 3.50)	3.02 (2.62, 3.33)	2.91 (2.60, 3.32)	**0.005**
Lesion length (mm)	20.40 (11.40, 32.40)	23.00 (12.80, 33.45)	18.90 (10.20, 32.00)	19.80 (11.40, 31.35)	0.142
Relative MLA (mm^2)	4.79 (3.67, 6.35)	5.29 (4.02, 6.98)	4.84 (3.63, 6.21)	4.37 (3.32, 5.86)	**<0.001**
Reference diameter (mm)	2.66 (1.69, 3.46)	2.58 (1.45, 3.48)	2.67 (1.77, 3.46)	2.74 (1.77, 3.46)	0.123
Average lumen area (mm^2)	6.42 (5.10, 8.00)	7.00 (5.60, 8.71)	6.40 (5.20, 7.78)	6.05 (4.59, 7.49)	**<0.001**
Average reference area (mm^2)	7.40 (6.17, 9.57)	7.67 (6.42, 10.08)	7.28 (6.00, 9.26)	7.18 (6.06, 9.40)	**0.029**
Lumen volume (mm^3)	137.50 (62.68, 237.12)	149.85 (71.60, 244.27)	130.75 (58.00, 240.53)	130.40 (62.15, 233.28)	0.332
Plaque burden (%)	50.60 (47.40, 54.10)	49.70 (46.98, 53.40)	50.70 (48.00, 54.30)	51.10 (47.52, 54.88)	**0.005**
Max. LCR	0.13 (0.10, 0.20)	0.13 (0.09, 0.19)	0.13 (0.10, 0.18)	0.14 (0.10, 0.22)	**0.026**
Symmetricity	0.80 (0.73, 0.86)	0.81 (0.74, 0.87)	0.81 (0.73, 0.86)	0.80 (0.72, 0.86)	0.081
Stent information					
Stent segment (mm)	33.20 (25.20, 43.00)	33.10 (25.40, 41.55)	34.00 (25.75, 45.40)	32.40 (24.40, 41.30)	0.132
Min stent area (mm^2)	4.97 (3.99, 6.28)	4.99 (3.99, 6.23)	5.00 (4.02, 6.48)	4.95 (3.86, 6.08)	0.656
Mean stent area (mm^2)	7.83 (6.46, 9.60)	7.87 (6.57, 9.69)	8.09 (6.60, 9.76)	7.55 (6.28, 9.19)	0.186
Min expansion (%)	64.00 (53.00, 75.00)	64.00 (53.00, 76.00)	65.00 (55.00, 75.25)	65.00 (52.25, 74.00)	0.892
Max expansion (%)	123.00 (111.00, 143.00)	121.00 (110.00, 140.00)	125.00 (112.00, 144.00)	125.00 (112.00, 144.00)	0.196
Mean expansion (%)	95.00 (86.00, 107.00)	95.00 (86.00, 105.00)	95.00 (86.00, 107.00)	97.00 (86.00, 108.00)	0.536
Plaque detection (interested segment)					
Plaque volume (mm^3)	134.10 (86.80, 190.50)	140.60 (91.23, 192.95)	130.25 (85.12, 192.80)	129.25 (84.75, 184.05)	0.437
Lipid plaque volume (mm^3)	10.16 (4.18, 19.66)	9.92 (3.85, 19.67)	9.94 (4.05, 19.07)	10.62 (4.63, 20.63)	0.383
Fibrous tissue volume (mm^3)	100.94 (59.67, 143.87)	106.46 (67.90, 147.84)	101.27 (55.99, 143.17)	94.86 (58.09, 140.03)	0.084
Calcification volume (mm^3)	0.51 (0.14, 1.62)	0.49 (0.11, 1.78)	0.51 (0.11, 1.73)	0.53 (0.18, 1.39)	0.775
Crystal volume (mm^3)	0.00 (0.00, 0.00)	0.00 (0.00, 0.00)	0.00 (0.00, 0.00)	0.00 (0.00, 0.00)	0.551
Macrophage volume (mm^3)	0.01 (0.00, 0.06)	0.01 (0.00, 0.05)	0.01 (0.00, 0.05)	0.01 (0.00, 0.07)	**0.048**
Max lipid area (mm^2)	2.33 (1.60, 3.03)	2.19 (1.52, 2.93)	2.29 (1.54, 3.07)	2.45 (1.71, 3.22)	**0.027**
Max lipid angle (°)	158.40 (120.00, 194.40)	155.85 (110.60, 191.10)	158.40 (120.17, 192.00)	162.65 (125.10, 201.00)	0.052
Thinnest cap (μm)	148 (111.00, 184.00)	155 (112.75, 188.00)	146 (114.00, 184.00)	144 (106.00, 177.00)	0.053
Max calcification area (mm^2)	0.61 (0.28, 1.09)	0.64 (0.25, 1.08)	0.61 (0.27, 1.09)	0.60 (0.31, 1.12)	0.932
Continued					

Variables	Total (*n* = 1056)	T1 (*n* = 340)	T2 (*n* = 362)	T3 (*n* = 354)	P value
Max calcification angle (°)	51.30 (32.20, 76.40)	46.30 (26.10, 76.40)	52.30 (32.70, 76.40)	52.30 (34.20, 76.40)	0.264
Post-procedural OFR					
Vessel-level OFR	0.92 (0.89, 0.95)	0.93 (0.90, 0.95)	0.93 (0.90, 0.95)	0.92 (0.89, 0.95)	**0.010**
Lesion residual OFR	0.98 (0.95, 1.00)	0.99 (0.96, 1.00)	0.98 (0.95, 1.00)	0.98 (0.95, 0.99)	**0.012**
Stent residual OFR	0.99 (0.97, 1.00)	0.99 (0.98, 1.00)	0.99 (0.97, 1.00)	0.99 (0.97, 1.00)	**0.037**

Table 2. Baseline pre-procedural coronary angiography, quantitative variables of post-procedural OCT and post-procedural vessel-level OFR. *OCT* optical coherence tomography, *OFR* optical flow ratio, *T1* tertile 1, *T2* tertile 2, *T3* tertile 3, *LAD* left anterior descending artery, *LCX* left circumflex artery, *RCA* right coronary artery, *MLA* minimum lumen area, *Max. LCR* maximum lipid-to-cap ratio. Bold values represent *P* < 0.05.

index, exhibited the highest c-index and incremental reclassification ability, as well as superior performance in identifying patients at risk for subsequent adverse cardiovascular events.

Subgroup analysis
Subgroup analysis was performed to assess the relationship between a prognostic model combining the TyG index and OFR. The risk score derived from the prognostic model, based on the TyG index and vessel-level OFR, was used to stratify patients into high- and low-risk groups. As shown in Table 4, the results of the subgroup analysis were consistent with the main findings of this study. In all subgroups, the incidence of MACE was higher in the high-risk group. Significant interactions were observed for dyslipidemia, right coronary artery (RCA) as the culprit vessel, and the model's interaction with MACE (*P* < 0.05). The predictive value of the model remained consistent across both diabetic and non-diabetic populations (*P* = 0.135).

Mediation analysis of vessel-level OFR for major adverse cardiovascular events in patients with ACS
A mediation analysis was conducted to assess the role of vessel-level OFR in the relationship between the TyG index and MACE in patients with ACS. In the crude model, the total effect of the TyG index on MACE was 0.117 (95% CI: 0.089–0.146, *P* < 0.05), with 17.9% of the TyG index's effect on MACE risk mediated through vessel-level OFR (indirect effect: 0.021, 95% CI: 0.011–0.034, *P* < 0.05). In Model 1, adjusted for traditional high-risk factors, the proportion mediated was 17.1%, with a total effect of 0.129 and an indirect effect of 0.022. In Model 2, which included additional adjustments for laboratory indices and angiographic data, the proportion mediated was 16.8%. The total effect increased to 0.137, while the indirect effect was 0.023. In Model 3, further adjusted for post-procedural OCT data, the proportion mediated decreased to 12.7%, with a total effect of 0.118 (*P* < 0.05) and an indirect effect of 0.015 (*P* < 0.05). This mediation analysis highlights that vessel-level OFR mediates the relationship between the TyG index and MACE. Although the proportion mediated decreases across progressively adjusted models, the role of vessel-level OFR as a mediator remains statistically significant. These findings suggest that a portion of the TyG index's effect on MACE is mediated indirectly through its impact on vessel-level OFR, emphasizing the mechanistic role of vessel-level OFR in linking the TyG index to adverse cardiovascular outcomes (Fig. 8).

Discussion
This study is the first to evaluate the relationship between the TyG index and OCT-derived computed physiological index, as well as its prognostic value in ACS patients. The novel findings include: (1) The TyG index is significantly correlated with vessel-level OFR measured immediately after procedure, and the relationship between the two is linear. (2) The TyG index is an independent predictor of MACE after procedure in ACS patients, with a non-linear association. (3) Vessel-level OFR independently predicts MACE risk in ACS patients and provides additional predictive value when combined with the TyG index.

Cardiovascular diseases (CVD) are the leading cause of death and morbidity globally, with a disproportionate burden in low- and middle-income countries. ACS is often the first clinical manifestation of CVD[26]. While controlling traditional risk factors has addressed some pathophysiological aspects of ACS, poor glycemic control remains a significant factor to ACS recurrence. IR is a hallmark of diabetes mellitus and is considered an independent risk factor for CVD[27]. Previous studies have demonstrated an association between HOMA-IR and myocardial injury, as well as clinical outcomes after PCI. IR was independently associated with elevated postoperative levels of troponin T and creatine kinase-MB, and with an increased risk of cardiovascular events during follow-up[28]. The TyG index, derived FBG and triglycerides, is a novel biomarker for assessing IR. It has been shown to outperform HOMA-IR in predicting IR[6–8].

Previous studies have demonstrated that the TyG index may be a useful marker for risk stratification and prognostication in patients with ACS, both with and without diabetes[9–12]. A retrospective cohort study of 2531 patients with diabetes and ACS and had 3 years of clinical follow-up revealed that an increase in the TyG index was associated with a higher incidence of MACE. After adjustment for traditional cardiovascular risk factors, the TyG index remained an independent predictor of MACE, regardless of whether patients received invasive treatment (HR: 1.455, 95% CI: 1.208–1.753)[9]. In a subsequent study, Ma et al. evaluated the role of the TyG index in predicting cardiovascular (CV) outcomes in patients with type 2 diabetes mellitus (T2DM) and ACS after PCI. Multivariate Cox proportional hazards regression, adjusted for multiple confounders, revealed a HR

of 2.17 (95% CI: 1.45–3.24; P for trend = 0.001) when comparing the highest and lowest tertiles of the TyG index. These findings suggest that the TyG index may be a useful predictor of CV outcomes after PCI[10]. Our study also demonstrated a nonlinear relationship between the TyG index and MACE (P for nonlinear < 0.021). Upon dividing patients into tertiles based on the TyG index, we observed that the cumulative incidence of MACE was significantly higher in those with a higher TyG index compared to those with a lower TyG index (all Log-rank P < 0.001).

ACS is often triggered by the rupture of vulnerable plaques, which are typically characterized by a large central lipid core, a high density of inflammatory cells, and a paucity of smooth muscle cells (SMCs). This has led to the concept of "vulnerable" or "high-risk" plaques, with the widely accepted hypothesis that coronary atherosclerotic instability results from the rupture of thin-cap fibroatheromas (TCFAs) due to collagen weakening mediated by inflammatory processes[29]. OCT is a catheter-based imaging technique that provides high-resolution, in vivo images of coronary arteries. Beyond morphological assessments, OCT can identify plaque composition by detecting lipid-rich plaques (LRPs) and measuring the thickness of the fibrous cap overlying the necrotic core. In clinical studies, the culprit lesions in ACS patients are often identified as LRPs and TCFAs, which are considered highly vulnerable to rupture[30]. In this study, we focused on the morphological characteristics of non-culprit plaques and their physiological parameters measured at different stages post-surgery. Significant differences in angiographic characteristics, including culprit vessel location were observed between groups. Post-procedural OCT analysis revealed that the proximal and distal reference diameters were the smallest, while the relative MLA, mean lumen area, and mean reference area were lowest in the high-TyG group. No significant differences in stent-related parameters were found between TyG tertiles. As the TyG index increased, parameters such as PB, LCR, and maximum lipid area of non-culprit lesions also increased. Additionally, OCT-detected macrophage volume was positively correlated with the TyG index. Elevated levels of the TyG index enhance macrophage accumulation, thereby increasing inflammatory activity within the arterial wall. Cytokines and enzymes, such as matrix metalloproteinases, released by macrophages contribute to the weakening of the fibrous cap, rendering the plaque more susceptible to rupture. Given that STEMI patients exhibit more severe coronary artery obstruction, the prognostic value of OFR in this group may be particularly significant. The TyG index is instrumental in identifying high-risk patients with metabolic abnormalities. In patients with chronic coronary syndrome (CCS), although the extent of coronary artery obstruction is generally less severe than in STEMI patients, metabolic abnormalities remain a critical risk factor. Zhao et al. demonstrated that the TyG index is a significant predictor of adverse outcomes in patients with T2DM and non-ST-segment elevation ACS after PCI[31]. Erdoğan et al. investigated the potential association between the TyG and the plasma atherogenic index (AIP) with MACE in patients with CCS. The study demonstrated that the TyG index is an independent predictor of MACE, with individuals having higher TyG levels exhibiting a significantly greater incidence of MACE. This suggests that the TyG index can serve as a predictive biomarker for adverse cardiovascular outcomes in CCS patients[32].

Previous studies have advanced the understanding of vulnerable plaques and inflammation from both mechanistic and therapeutic perspectives. However, most plaque ruptures are subclinical, with no overt clinical manifestations. Thus, the occurrence of acute coronary events also depends on hemodynamic changes. The invasive physiological index FFR reflects the severity of atherosclerotic disease and provides prognostic value. Ahn et al. aimed to assess the prognostic value of deferred FFR measurement and its relationship with coronary artery stenosis following revascularization. they concluded that FFR values are linearly correlated with cardiac event risk. Li et al. investigated the predictive value of FFR after procedure for target vessel failure (TVF) over a 1- to 3-year period. The study found that FFR ≤ 0.88 after DES was closely related to TVF and was the only predictor of TVF[33]. Subsequently, Hwang et al. developed a risk model integrating clinical, angiographic, and physiological parameters to predict future clinical events after DES. The study found that a risk model combining these parameters more accurately predicted the risk of TVF within 2 years, with total stent length and post-PCI FFR being the most important predictors[34]. Additionally, The high TyG group had significantly lower vessel-level OFR, lesion residual OFR, and stent residual OFR, suggesting impaired coronary physiological function.

AI-based computational algorithms have been developed to accurately assess coronary physiology and plaque morphology. These approaches offer fully automated and comprehensive morphofunctional evaluations of coronary plaques, enhancing reproducibility and minimizing subjectivity in assessments[21]. The OFR is a computational physiological index calculated by the AI software, which employs a deep learning algorithm. OFR demonstrates a significantly stronger correlation with wire-based FFR than traditional measurements, such as minimum lumen area or percent area stenosis assessed using OCT[16–19]. Kakizaki et al. investigated the relationship between OCT-derived FFR and long-term cardiovascular outcomes after PCI in patients with ACS. They found that low vessel-level OCT-FFR (< 0.90) was an independent predictor of TVF and that adding OCT-FFR measurements to post-PCI OCT results improved the discrimination of patients at risk for subsequent TVF[22]. Hong et al. combined plaque morphology and computational physiology to assess the predictive value of MACE in patients with ACS. They found that LCR and OFR were superior to MLA in predicting 2-year non-culprit vessel-related MACE. Furthermore, the combination of LCR and OFR identified a subgroup of patients with a 43-fold increased risk of cardiovascular events. The study also showed that the combination of TCFA and OFR identified patients at higher risk of future events[21].

Our study confirms that lower vessel-level OFR is associated with an increased risk of MACE. Additionally, we observed a linear relationship between the TyG index and post procedural vessel-level OFR, with a progressive decline in physiological parameters as the TyG index increased. Notably, we found that TyG, as an independent risk factor, when combined with vessel-level OFR, yielded the highest C-index and demonstrated superior incremental reclassification ability. The combination of TyG and vessel-level OFR effectively identified patient subgroups at high risk for cardiovascular events. This model outperformed either factor alone in identifying patients at risk for subsequent adverse cardiovascular events. Furthermore, it was applicable across
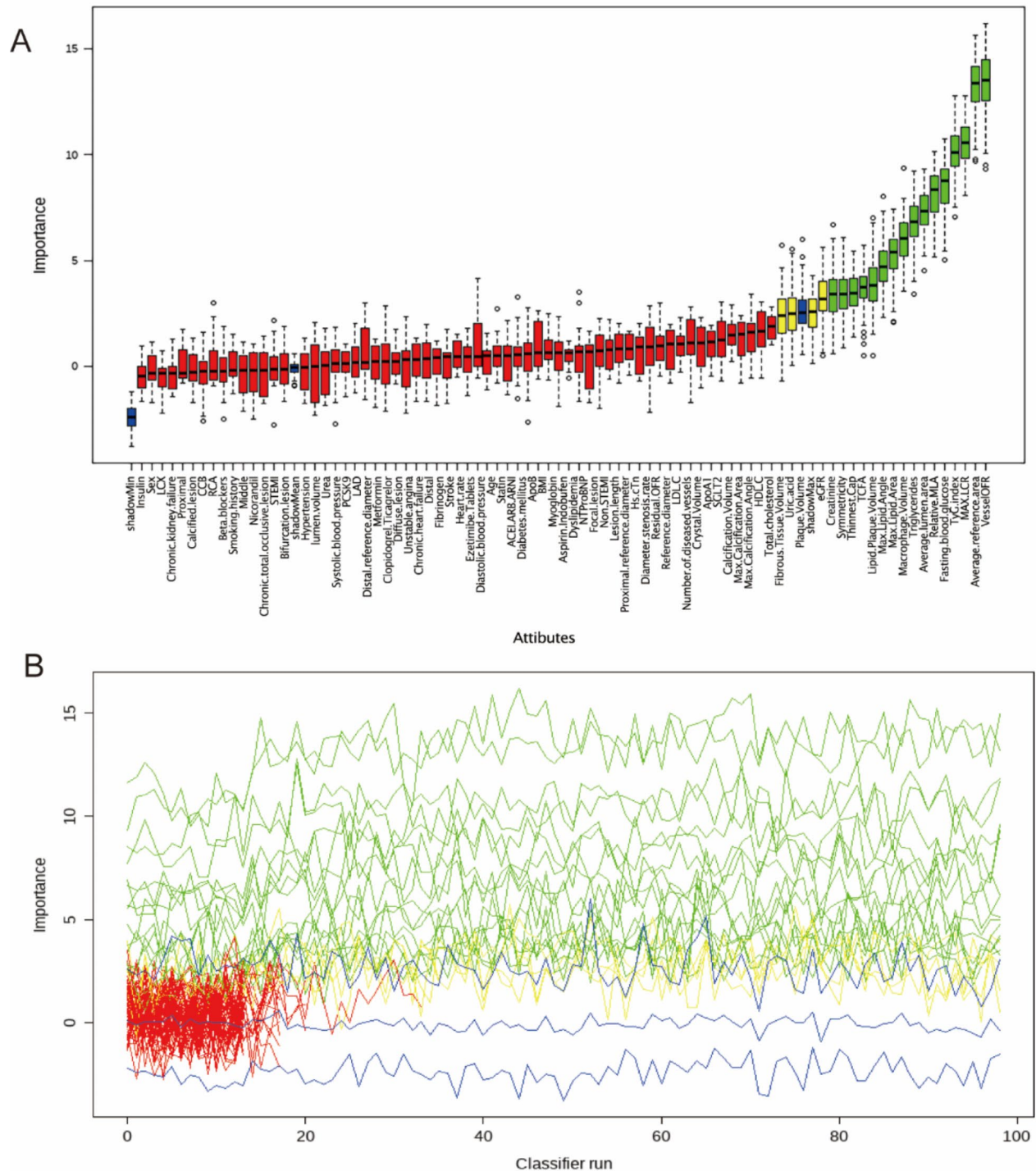
different clinical phenotypes of ACS, as well as in both diabetic and non-diabetic populations. This study also elucidates the correlation and mediating role of vessel-level OFR in the relationship between TyG index and adverse cardiovascular outcomes, thereby integrating prior evidence into a holistic pathway that informs clinical decision making.

Overall, our study elucidates the emerging role of the OCT-derived computational physiological index in patients with ACS after PCI, highlighting its correlation and additive predictive value. Furthermore, we show that the vessel-level OFR mediates the relationship between the TyG index and MACE. Integration of these indices can be used for risk stratification and prognostic prediction in ACS patients. The integration of the TyG index and OFR into clinical practice provides a valuable tool for both primary and secondary prevention of cardiovascular events in ACS patients. In primary prevention, the TyG index serves as an early marker to identify individuals at high risk of developing ACS, particularly in populations with a high prevalence of

◀**Fig. 3**. Feature selection of potential factors associated with the MACE using the Boruta algorithm. Process of feature selection. B. Evolution of Z-scores during the selection process. The x-axis in (**A**, **B**) represents the variable names and the number of iterations, respectively. The y-axis indicates the Z-value for each variable. Blue boxes and lines correspond to the minimum, average, and maximum Z-scores for shadow features. Green boxes and lines represent confirmed variables, yellow indicates tentative features, and red denotes variables rejected by the model during computation. *LCX* left circumflex artery, *CCB* calcium channel blocker, *RCA* right coronary artery, *STEMI* ST-Elevation Myocardial Infarction, *PCSK9* proprotein convertase subtilisin/kexin type 9, *LAD* left anterior descending artery, *ACEI/ARB/ARNI* angiotensin-converting enzyme inhibitors/angiotensin receptor blockers/angiotensin receptor-neprilysin inhibitors, *APOB* Apolipoprotein B, *BMI* body mass index, *NTproBNP* N-terminal pro B-type natriuretic peptide, *OFR* optical flow Ratio, *LDL-C* low-density lipoprotein cholesterol, *APOA1* Apolipoprotein A1, *SGLT2* sodium-glucose cotransporter 2 inhibitors, *HDL-C* high-density lipoprotein cholesterol, *eGFR* estimated glomerular filtration rate, *TCFA* thin-cap fibroatheroma, *MLA* minimum lumen area, *LCR* lipid-to-cap ratio.
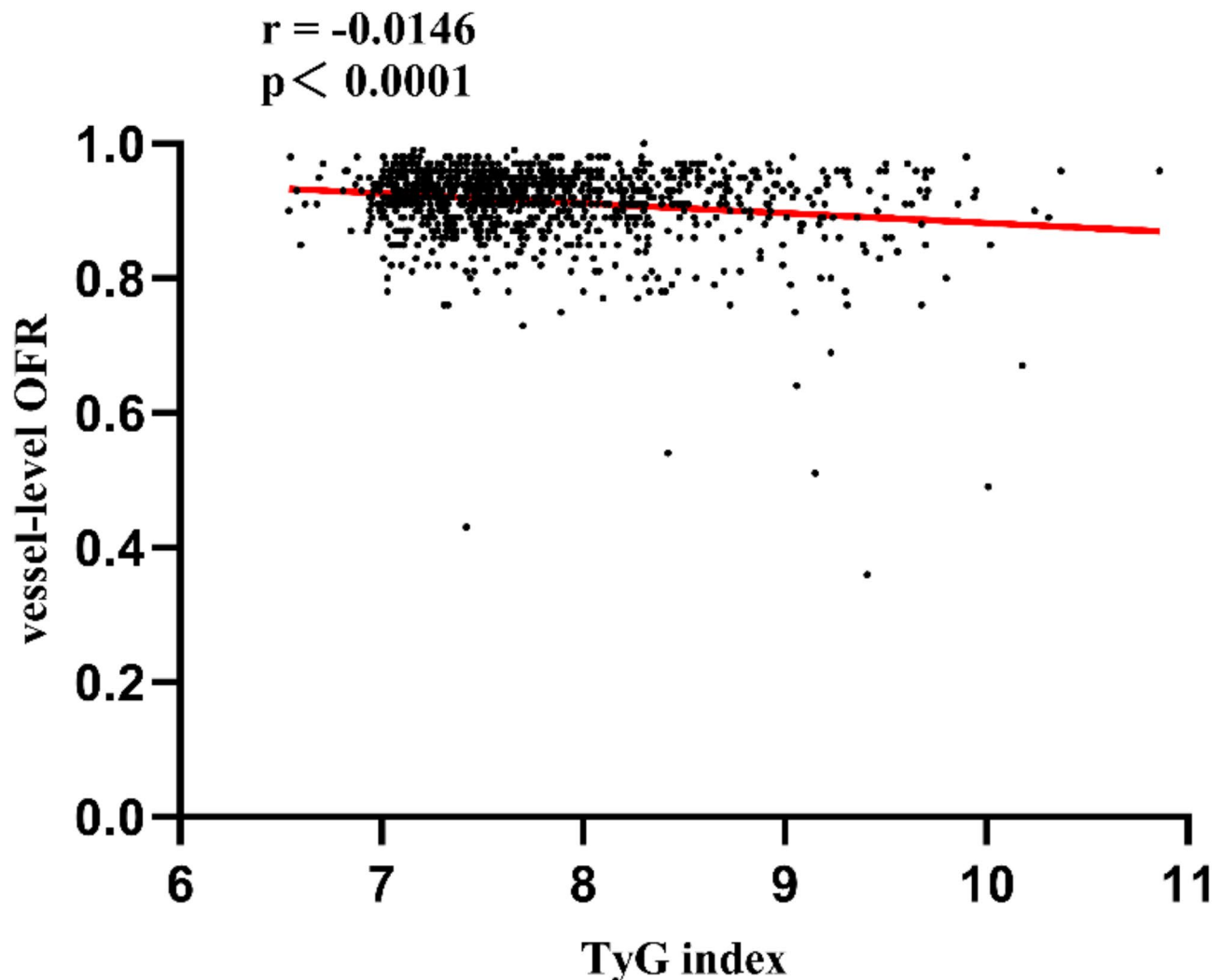

Fig. 4. Correlation between the TyG index and vessel-level OFR in ACS patients. The correlation between the TyG index and vessel-level OFR in ACS patients was assessed using Spearman's rank correlation test. The results demonstrate an inverse correlation between the TyG index and vessel-level OFR. *ACS* acute coronary syndrome, *TyG* triglyceride-glucose, *OFR* optical flow ratio.

diabetes and insulin resistance. Monitoring the TyG index in these individuals can guide lifestyle modifications and pharmacological interventions to improve insulin sensitivity and reduce cardiovascular risk. For secondary prevention, the combined use of the TyG index and OFR significantly enhances risk stratification following PCI. Patients presenting with a high TyG index and a low OFR post-PCI may necessitate more aggressive management strategies, including intensive glycemic control, lipid-lowering therapy, and closer follow-up. This combination of indices also facilitates personalized treatment approaches, optimizes stent placement strategies,
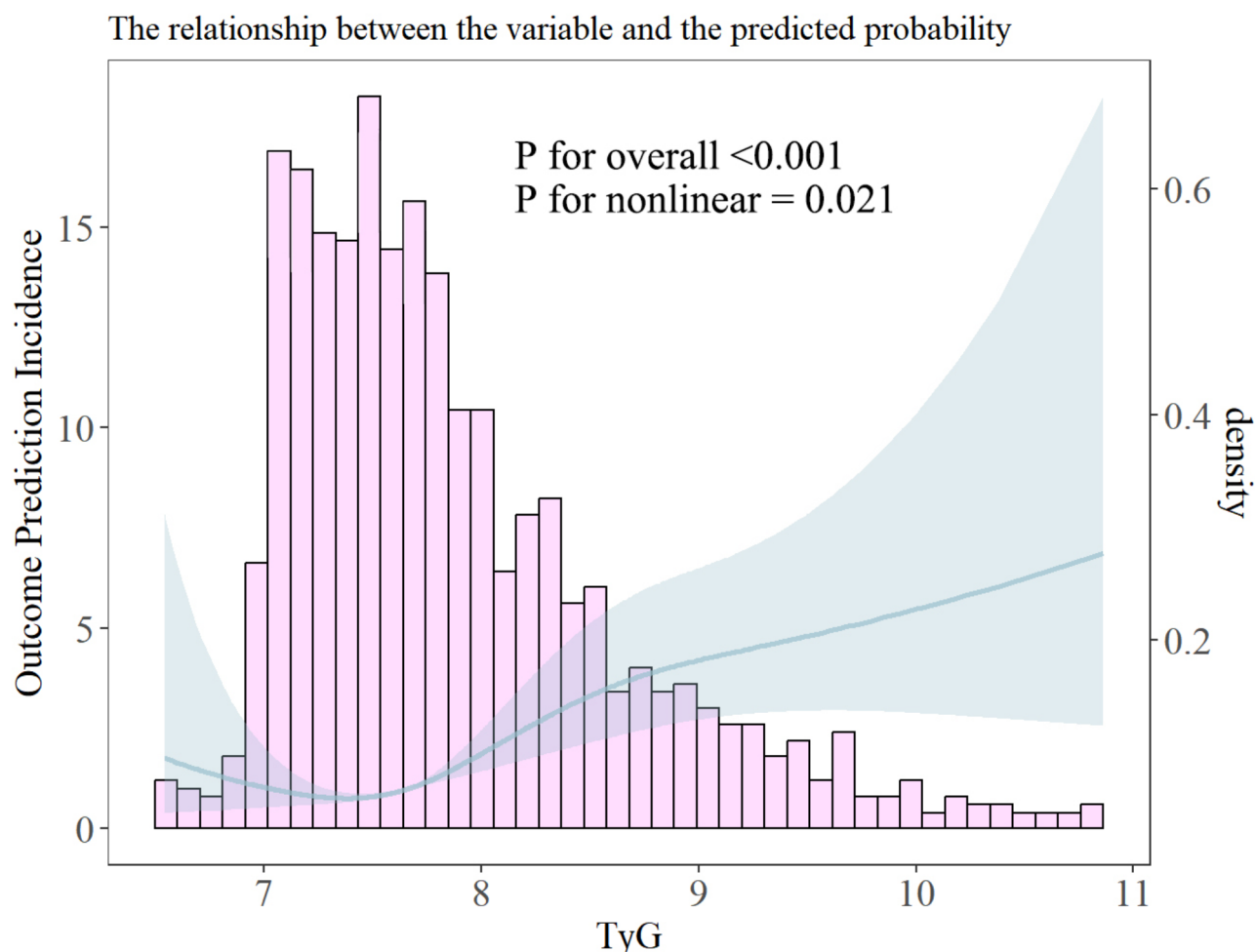
Fig. 5. Multivariate RCS regression analysis for the nonlinear association between the TyG index and MACE in ACS patients. A multivariate RCS analysis was performed to investigate both linear and nonlinear associations between the TyG index and endpoints in ACS patients post-PCI. The RCS model revealed a nonlinear relationship between the TyG index and the probability of MACE. *TyG* triglyceride-glucose, *RCS* restricted cubic splines, *MACE* major adverse cardiovascular events, *HR* hazard ratio, *CI* confidence interval.

and may inform the need for additional intracoronary imaging or PCI. Although our findings were validated in the Asian population, we recognize the importance of further studies in non-Asian populations and in patients with different ACS phenotypes. To improve the global relevance of the study, we call for further multicenter studies in patients of different races, ethnicities and ACS phenotypes. This will help to validate our findings and determine the applicability and prognostic value of the TyG index and OFR combination in a broader population.

Study limitations
This study has several limitations. First, it was a single-center, retrospective analysis, which may have introduced confounding factors related to the presence of disease. Although we adjusted for these confounders in our model to minimize bias, residual selection bias may still exist. Second, the TyG index was assessed only once at admission, and its fluctuations during follow-up were not measured or analyzed. Third, the absence of large randomized controlled trials investigating the prognostic value of vessel-level OFR in ACS patients, combined with our findings validated solely in an Asian population, underscores the need for multicenter studies encompassing various races, ethnicities, and ACS phenotypes to rigorously assess the broader applicability and prognostic value of the TyG index and OFR combination, and to validate the correlation between insulin resistance and computational physiology suggested by our exploratory study.

Conclusion
In this study, we demonstrated the correlation between the TyG index and vessel-level OFR, and the mediating role of vessel-level OFR between the TyG index and MACE, with the association between TyG and MACE being non-linear. Ultimately, we found that combining the TyG index and vessel-level OFR effectively identifies a subgroup of high-risk patients for cardiovascular events.
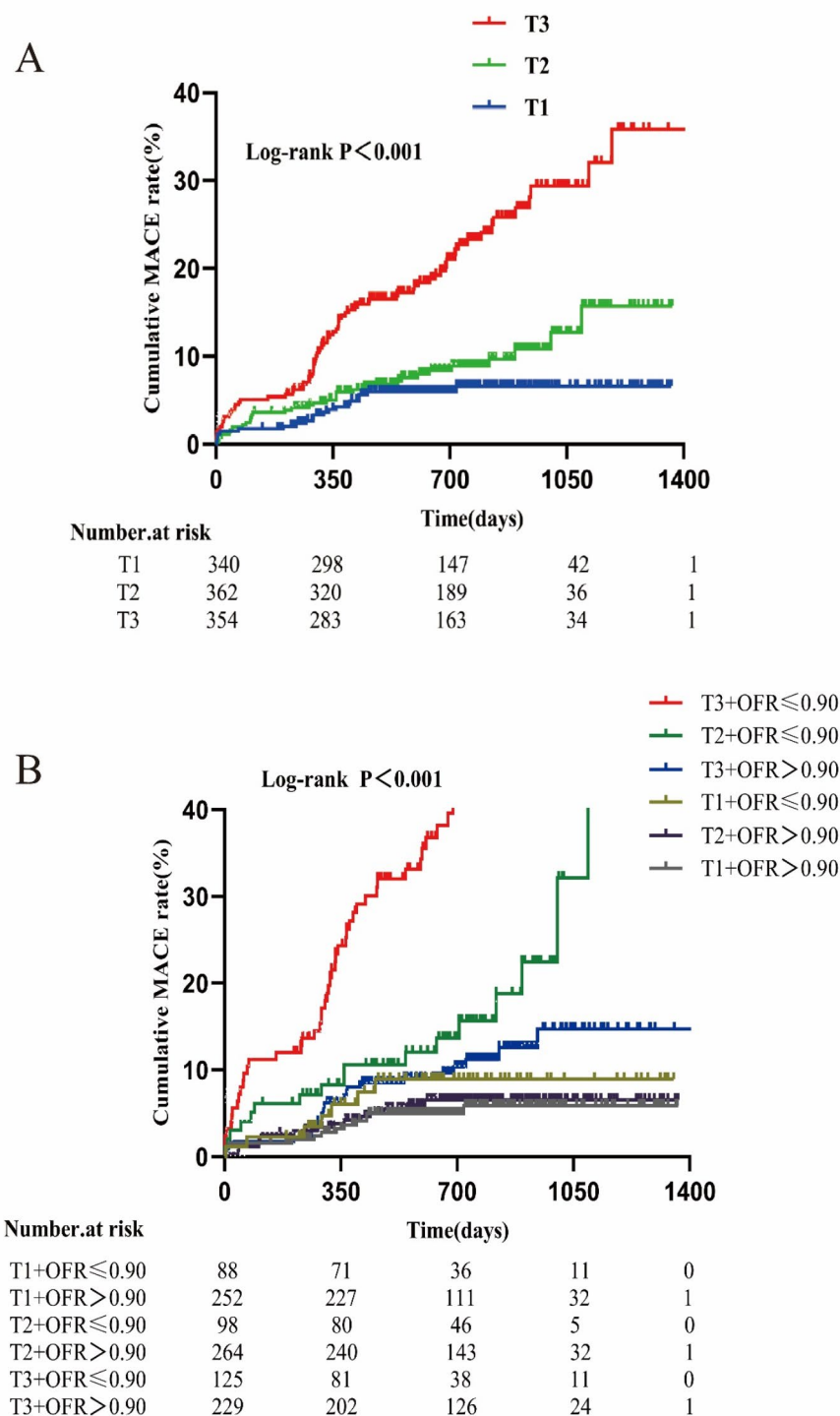
Fig. 6. Kaplan-Meier curves for MACE based on TyG tertiles and combined TyG tertiles with OFR. Participants were stratified into three groups based on the TyG index: T1 (TyG index < 7.42), T2 (7.42 ≤ TyG index < 7.95), and T3 (TyG index ≥ 7.95). Kaplan-Meier survival curves demonstrated that the cumulative incidence of MACE was significantly higher in patients with elevated TyG indices. Furthermore, when stratified by both TyG index and vessel-level OFR, the incidence of MACE was markedly higher in patients with a combination of high TyG index and low postoperative vessel-level OFR. (**A**) Kaplan-Meier curves for MACE grouped by the TyG index tertiles. (**B**) Kaplan-Meier curves for MACE grouped by the TyG index tertiles and vessel-level OFR levels (categorized by a cutoff value of 0.90). *TyG* triglyceride-glucose, *MACE* major adverse cardiovascular events, *OFR* optical flow ratio.

	Crude model HR (95% CI)	P value	Model 1 HR (95% CI)	P value	Model 2 HR (95% CI)	P value	Model 3 HR (95% CI)	P value
Vessel-level OFR (per 0.1 increase)	0.560 (0.481, 0.652)	<0.001	0.551 (0.468, 0.648)	<0.001	0.557 (0.468, 0.662)	<0.001	0.734(0.598,0.900)	0.003
TyG index	2.149 (1.762, 2.622)	<0.001	2.324 (1.882, 2.870)	<0.001	2.523 (2.015, 3.159)	<0.001	2.279(1.798,2.889)	<0.001
TyG tertiles								
T1	1 (reference)		1 (reference)		1 (reference)		1 (reference)	
T2	1.268 (0.130, 12.418)	0.838	1.708 (0.180, 16.223)	0.641	1.953 (0.194, 19.696)	0.570	5.342(0.453,63.058)	0.183
T3	1.760 (1.239, 2.501)	0.002	1.704 (1.178, 2.465)	0.005	1.912 (1.253, 2.917)	0.003	1.666(1.054,2.634)	0.029
P for trend		<0.001		<0.001		<0.001		<0.001
Crude mode	Unadjusted							
Model 1	Adjusted for age>65y, hypertension, diabetes mellitus, dyslipidemia, smoking history							
Mode 2	Adjusted for age>65y, hypertension, diabetes mellitus, dyslipidemia, smoking history, diameter stenosis rate, sex, BMI, SBP, DBP, total cholesterol, LDL-C, uric acid, NTProBNP, Hsc-Tn							
Mode 3	Adjusted for Age>65y, hypertension, diabetes mellitus, dyslipidemia, smoking history, diameter stenosis rate, sex, BMI, SBP, DBP, total cholesterol, LDL-C, uric acid, NTProBNP, Hsc-Tn, maximum lipid angle, MAX.LCR, symmetricity, lumen volume, lesion length							

Table 3. The association between various TyG index groups and vessel-level OFR and endpoints. HR corresponds to an increase of 1 unit for each variable except for OFR. *TyG* triglyceride-glucose, *OFR* optical flow ratio, *HR* hazard ratio, *CI* confidence interval, *T1* tertile 1, *T2* tertile 2, *T3* tertile 3, *BMI* body mass index, *SBP* systolic blood pressure, *DBP* diastolic blood pressure, *LDL-C* low-density lipoprotein cholesterol, *NTproBNP* N-terminal pro B-type natriuretic peptide, *Hs-cTn* high-sensitivity cardiac troponin, *MAX.LCR* maximum lipid-to-cap ratio.
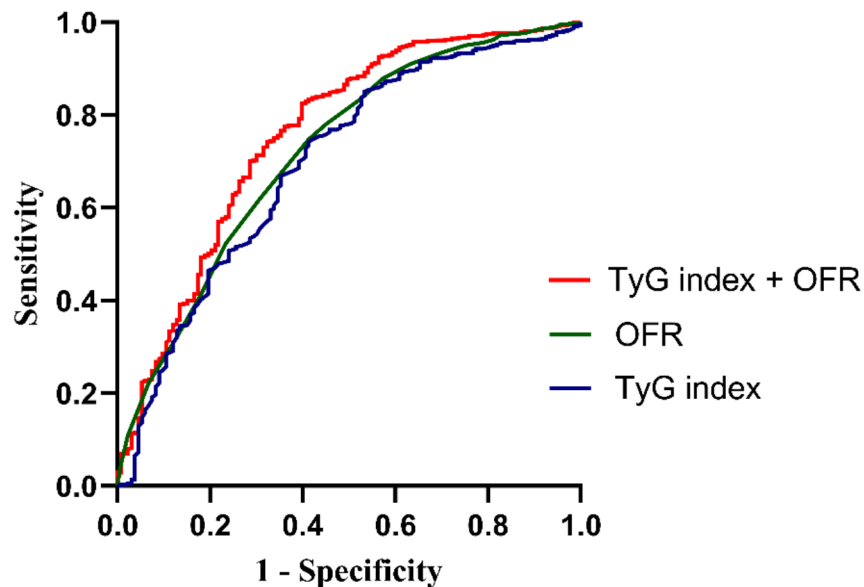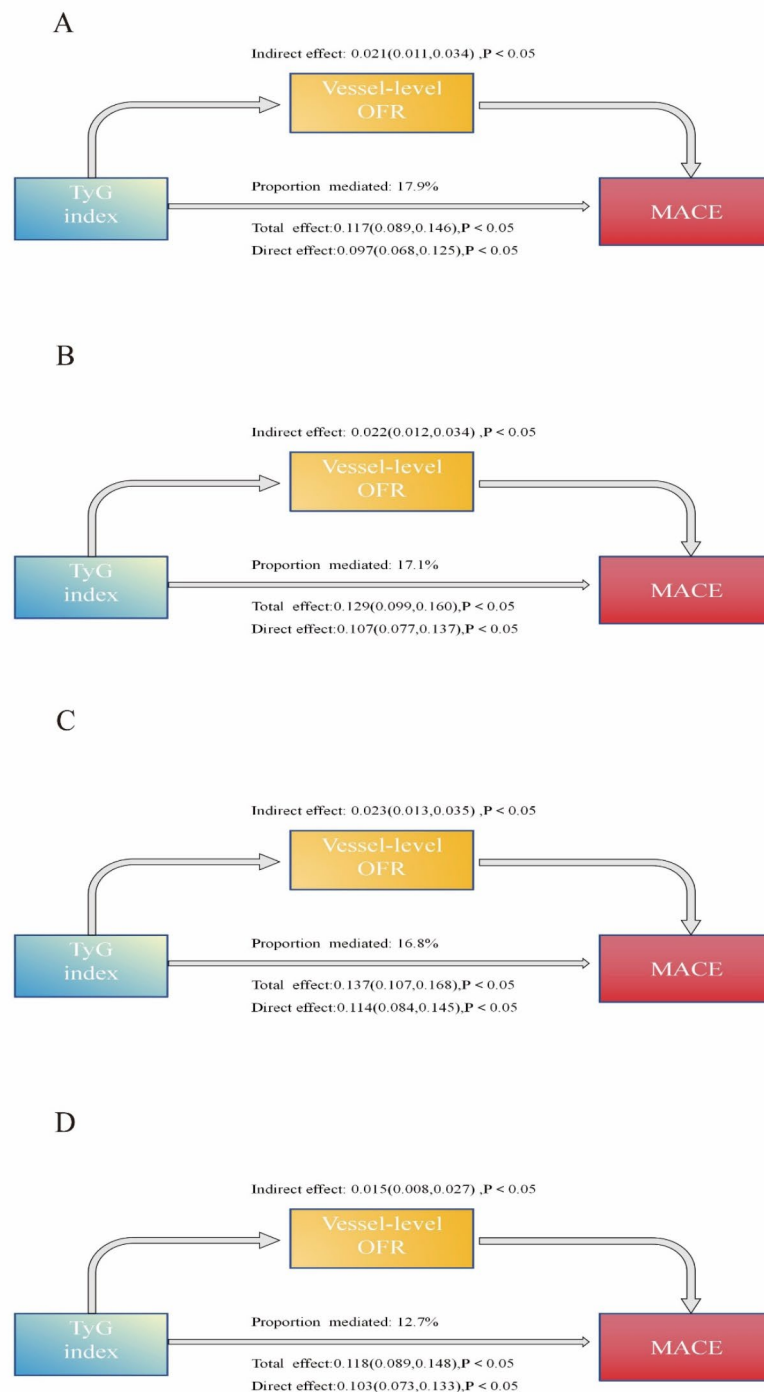
Prediction Model	C-index	P value	NRI	P value	IDI	P value
TyG index	0.697					
OFR	0.720					
TyG index + OFR	0.757	VS OFR	VS OFR	VS OFR	VS OFR	VS OFR
		< 0.001	0.373	< 0.001	0.031	< 0.001

Fig. 7. Discriminatory and Reclassification ability of predictive models for MACE. The figure above displays the ROC curves for predicting MACE using the TyG index, vessel-level OFR, and their combination. Compared to model 1 (vessel-level OFR), model 2 (model 1 plus TyG) demonstrated significantly higher discriminatory power and reclassification ability in identifying ACS patients for subsequent MACE. *TyG* triglyceride-glucose, *MACE* major adverse cardiovascular events, *OFR* optical flow ratio, *ACS* acute coronary syndrome, *ROC* receiver operating characteristic, *IDI* integrated discrimination improvement, *NRI* net reclassification index.

Variables	Patients, *n* (%)	Low risk	High risk	HR (95% CI)	*P* for trend	*P* for interaction
Age ≥ 65 years						0.254
No	683 (64.68)	30/522	55/161	7.40 (4.72–11.61)	< 0.001	
Yes	373 (35.32)	23/293	25/80	4.54 (2.58–8.00)	< 0.001	
Hypertension						0.686
No	472 (44.70)	26/367	35/105	5.89 (3.52–9.85)	< 0.001	
Yes	584 (55.30)	27/448	45/136	6.53 (4.05–10.54)	< 0.001	
Diabetes mellitus						0.135
No	836 (79.17)	47/665	57/171	5.54 (3.76–8.16)	< 0.001	
Yes	220 (20.83)	6/150	23/70	12.24 (4.64–32.29)	< 0.001	
Dyslipidemia						0.008
No	823 (77.94)	50/656	53/167	4.86 (3.30–7.16)	< 0.001	
Yes	233 (22.06)	3/159	27/74	38.17 (9.07–160.73)	< 0.001	
Smoke						0.977
No	514 (48.67)	29/400	40/114	6.19 (3.81–10.05)	< 0.001	
Yes	542 (51.33)	24/415	40/127	6.24 (3.76–10.36)	< 0.001	
Male						0.181
No	175 (16.57)	14/130	15/45	3.82 (1.84–7.93)	< 0.001	
Yes	881 (83.43)	39/685	65/196	7.09 (4.75–10.58)	< 0.001	
BMI ≥ 24 kg/m^2						0.619
No	497 (47.06)	23/402	30/95	6.66 (3.86–11.48)	< 0.001	
Yes	559 (52.94)	30/413	50/146	5.75 (3.64–9.10)	< 0.001	
Clinical presentation						
STEMI						0.945
No	627 (59.38)	28/493	39/134	6.20 (3.81–10.08)	< 0.001	
Yes	429 (40.62)	25/322	41/107	5.92 (3.58–9.81)	< 0.001	
NSTEMI						0.075
No	821 (77.75)	40/633	70/188	7.20 (4.86–10.65)	< 0.001	
Yes	235 (22.25)	13/182	10/53	3.05 (1.33–6.98)	0.008	
UA						0.205
No	666 (63.07)	38/504	53/162	5.21 (3.42–7.94)	< 0.001	
Yes	390 (36.93)	15/311	27/79	8.42 (4.48–15.83)	< 0.001	
Target vessel						
LAD						0.010
No	551 (52.18)	22/458	34/93	10.04 (5.82–17.33)	< 0.001	
Yes	505 (47.82)	31/357	46/148	4.08 (2.58–6.43)	< 0.001	
LCX						0.728
No	881 (83.43)	45/672	69/209	6.06 (4.15–8.84)	< 0.001	
Yes	175 (16.57)	8/143	11/32	7.19 (2.89–17.90)	< 0.001	
RCA						0.016
No	680 (64.39)	39/500	57/180	4.65 (3.09–6.99)	< 0.001	
Yes	376 (35.61)	14/315	23/61	11.92 (6.01–23.65)	< 0.001	
Lesion segment						
Proximal						0.562
No	678 (64.20)	33/533	50/145	6.69 (4.31–10.40)	< 0.001	
Yes	378 (35.80)	20/282	30/96	5.48 (3.08–9.76)	< 0.001	
Middle						0.322
Continued						

Variables	Patients, *n* (%)	Low risk	High risk	HR (95% CI)	*P* for trend	*P* for interaction
No	515 (48.77)	31/404	38/111	5.31 (3.29–8.57)	<0.001	
Yes	541 (51.23)	22/411	42/130	7.39 (4.40–12.39)	<0.001	
Distal						0.584
No	894 (84.66)	42/684	69/210	6.55 (4.44–9.64)	<0.001	
Yes	162 (15.34)	11/131	11/31	5.27 (2.28–12.19)	<0.001	

Table 4. Cox proportional hazards analysis was performed to evaluate the combination of the TyG index and vessel-level OFR across different subgroups. *HR* hazard ratio, *CI* confidence interval, *BMI* body mass index, *STEMI* ST-segment elevation myocardial infarction, *UA* unstable angina, *LAD* left anterior descending artery, *LCX* left circumflex artery, *RCA* right coronary artery. The risk score, derived from the prognostic model that combines the TyG index and vessel-level OFR, was categorized into high-risk and low-risk groups. This categorization was used to assess whether the model's prognostic value differed across various subgroups, while also calculating the interaction P-value.

A

Indirect effect: 0.021(0.011,0.034) ,P < 0.05

Vessel-level OFR

TyG index

Proportion mediated: 17.9%

MACE

Total effect:0.117(0.089,0.146),P < 0.05
Direct effect:0.097(0.068,0.125),P < 0.05

B

Indirect effect: 0.022(0.012,0.034) ,P < 0.05

Vessel-level OFR

TyG index

Proportion mediated: 17.1%

MACE

Total effect:0.129(0.099,0.160),P < 0.05
Direct effect:0.107(0.077,0.137),P < 0.05

C

Indirect effect: 0.023(0.013,0.035) ,P < 0.05

Vessel-level OFR

TyG index

Proportion mediated: 16.8%

MACE

Total effect:0.137(0.107,0.168),P < 0.05
Direct effect:0.114(0.084,0.145),P < 0.05

D

Indirect effect: 0.015(0.008,0.027) ,P < 0.05

Vessel-level OFR

TyG index

Proportion mediated: 12.7%

MACE

Total effect:0.118(0.089,0.148),P < 0.05
Direct effect:0.103(0.073,0.133),P < 0.05

◄ **Fig. 8.** Decomposition of the total association of the TyG index and MACE. In different adjusted models, the total association between the TyG index and post-procedure MACE in ACS patients was decomposed into direct and indirect associations mediated by vessel-level OFR. All effects are represented by β coefficients. *TyG* triglyceride-glucose, *MACE*: major adverse cardiovascular events, *OFR* optical flow ratio, *HR* hazard ratio, *CI* confidence interval, *PM* proportion mediated, *BMI* body mass index, *NTproBNP* N-terminal pro B-type natriuretic peptide, *SBP* systolic blood pressure, *DBP* diastolic blood pressure, *LDL-C* low-density lipoprotein cholesterol, *Hs-cTn* high-sensitivity cardiac troponin, *MAX.LCR* maximum lipid-to-cap ratio. A represents the crude model; B represents the adjusted Model 1; C represents the adjusted Model 2; D represents the adjusted Model 3. Crude model: unadjusted; Model 1: adjusted for age > 65 years, hypertension, diabetes mellitus, dyslipidemia, and smoking history; Model 2: Model 1 adjusted for diameter stenosis rate, sex, BMI, SBP, DBP, total cholesterol, LDL-C, uric acid, NTProBNP, and Hs-cTn; Model 3: Model 2 adjusted for maximum lipid angle, maximum lipid-to-cap ratio, symmetry, lumen volume, and lesion length.

Data availability

The datasets generated during the current study are not publicly available due to privacy and ethical constraints but can be obtained from the corresponding author on reasonable request.

References
1. Ralapanawa, U. & Sivakanesan, R. Epidemiology and the magnitude of coronary artery disease and acute coronary syndrome: a narrative review. *J. Epidemiol. Global Health.* **11**, 169–177 (2021).
2. Sabatine, M. S. et al. Evolocumab and clinical outcomes in patients with cardiovascular disease. *N Engl. J. Med.* **376**, 1713–1722 (2017).
3. Cannon, C. P. et al. Ezetimibe added to Statin therapy after acute coronary syndromes. *N Engl. J. Med.* **372**, 2387–2397 (2015).
4. Hill, M. A. et al. Insulin resistance, cardiovascular stiffening and cardiovascular disease. *Metab. Clin. Exp.* **119**, 154766 (2021).
5. Minh, H. V. et al. Assessment of preferred methods to measure insulin resistance in Asian patients with hypertension. *J. Clin. Hypertens. (Greenwich Conn).* **23**, 529–537 (2021).
6. Simental-Mendía, L. E., Rodríguez-Morán, M. & Guerrero-Romero, F. The product of fasting glucose and triglycerides as surrogate for identifying insulin resistance in apparently healthy subjects. *Metab. Syndr. Relat. D.* **6**, 299–304 (2008).
7. Tao, L. C., Xu, J. N., Wang, T. T., Hua, F. & Li, J. J. Triglyceride-glucose index as a marker in cardiovascular diseases: landscape and limitations. *Cardiovasc. Diabetol.* **21**, 68 (2022).
8. Liu, M. et al. Triglyceride-glucose body mass index predicts prognosis in patients with ST-elevation myocardial infarction. *Sci. Rep.* **14**, 976 (2024).
9. Wang, L. et al. Triglyceride-glucose index predicts adverse cardiovascular events in patients with diabetes and acute coronary syndrome. *Cardiovasc. Diabetol.* **19**, 80 (2020).
10. Ma, X. et al. The effect of HsCRP on TyG index-associated cardiovascular risk in patients with acute coronary syndrome undergoing PCI. *Sci. Rep.* **14**, 18083 (2024).
11. Cai, X. L. et al. Prognostic value of triglyceride glucose index in population at high cardiovascular disease risk. *Cardiovasc. Diabetol.* **22**, 198 (2023).
12. Wang, W. et al. Association between the triglyceride-glucose index and in-hospital major adverse cardiovascular events in patients with acute coronary syndrome: results from the improving care for cardiovascular disease in China (CCC)-acute coronary syndrome project. *Cardiovasc. Diabetol.* **23**, 170 (2024).
13. Dauerman, H. L. Optical coherence tomography—light and truth. *N Engl. J. Med.* **389**, 1523–1525 (2023).
14. Niioka, H. et al. Automated diagnosis of optical coherence tomography imaging on plaque vulnerability and its relation to clinical outcomes in coronary artery disease. *Sci. Rep.* **12**, 14067 (2022).
15. Zhao, X. et al. Triglyceride glucose index combined with plaque characteristics as a novel biomarker for cardiovascular outcomes after percutaneous coronary intervention in ST-elevated myocardial infarction patients: an intravascular optical coherence tomography study. *Cardiovasc. Diabetol.* **20**, 131 (2021).
16. Chu, M. et al. Artificial intelligence and optical coherence tomography for the automatic characterisation of human atherosclerotic plaques. *EuroIntervention* **17**, 41–50 (2021).
17. Hu, F. et al. Diagnostic accuracy of optical flow ratio: an individual patient-data meta-analysis. *EuroIntervention* **19**, e145–e154 (2023).
18. Yu, W. et al. Diagnostic accuracy of intracoronary optical coherence tomography-derived fractional flow reserve for assessment of coronary stenosis severity. *EuroIntervention* **15**, 189–197 (2019).
19. Huang, J. et al. Diagnostic performance of intracoronary optical coherence tomography-based versus angiography-based fractional flow reserve for the evaluation of coronary lesions. *EuroIntervention* **16**, 568–576 (2020).
20. Gessert, N. et al. Automatic plaque detection in IVOCT pullbacks using convolutional neural networks. *IEEE Trans. Med. Imaging.* **38**, 426–434 (2019).
21. Hong, H. et al. Risk stratification in acute coronary syndrome by comprehensive morphofunctional assessment with optical coherence tomography. *JACC Asia.* **2**, 460–472 (2022).
22. Kakizaki, S. et al. Optical coherence tomography fractional flow reserve and cardiovascular outcomes in patients with acute coronary syndrome. *JACC Cardiovasc. Interv.* **15**, 2035–2048 (2022).
23. Otsuka, K. et al. Impact of diabetes mellitus and triglyceride glucose index on mortality and cardiovascular outcomes in patients with chronic coronary syndrome undergoing coronary computed tomography angiography. *Int. J. Cardiol. Cardiovasc. Risk Prev.* **20**, 200250 (2024).
24. Nakanishi, K. et al. Prognostic value of coronary flow reserve on long-term cardiovascular outcomes in patients with chronic kidney disease. *Am. J. Cardiol.* **112**, 928–932 (2013).
25. Thygesen, K. et al. Fourth universal definition of myocardial infarction (2018). *J. Am. Coll. Cardiol.* **72**, 2231–2264 (2018).
26. GBD 2019 Diseases and Injuries Collaborators. Global burden of 369 diseases and injuries in 204 countries and territories, 1990–2019: a systematic analysis for the global burden of disease study 2019. *Lancet* **396**, 1204–1222 (2020).
27. Laakso, M. & Kuusisto, J. Insulin resistance and hyperglycaemia in cardiovascular disease development. *Nat. Rev. Endocrinol.* **10**, 293–302 (2014).

28. Uetani, T. et al. Impact of insulin resistance on post-procedural myocardial injury and clinical outcomes in patients who underwent elective coronary interventions with drug-eluting stents. *JACC Cardiovasc. Interv.* **5**, 1159–1167 (2012).
29. Finn, A. V., Nakano, M., Narula, J., Kolodgie, F. D. & Virmani, R. Concept of vulnerable/unstable plaque. *Arterioscler. Thromb. Vasc Biol.* **30**, 1282–1292 (2010).
30. Yabushita, H. et al. Characterization of human atherosclerosis by optical coherence tomography. *Circulation* **106**, 1640–1645 (2002).
31. Zhao, Q. et al. Impacts of triglyceride-glucose index on prognosis of patients with type 2 diabetes mellitus and non-ST-segment elevation acute coronary syndrome: results from an observational cohort study in China. *Cardiovasc. Diabetol.* **19**, 108 (2020).
32. Erdoğan, A. et al. The triglyceride-glucose index might be a better indicator for predicting poor cardiovascular outcomes in chronic coronary syndrome. *J. Clin. Med.* **12**, 6201 (2023).
33. Li, S. J. et al. Cutoff value and long-term prediction of clinical events by FFR measured immediately after implantation of a drug-eluting stent in patients with coronary artery disease: 1- to 3-year results from the DKCRUSH VII registry study. *JACC Cardiovasc. Interv.* **10**, 986–995 (2017).
34. Hwang, D. et al. Role of post-stent physiological assessment in a risk prediction model after coronary stent implantation. *JACC Cardiovasc. Interv.* **13**, 1639–1650 (2020).

Author contributions

Li Pan: Design, Supervision, Writing; Original Draft Preparation; Shiwan Lu: Formal Analysis; Qianhang Xia: Design, Methodology; Yi Deng: Formal Analysis, validation; Shitao Luo: Conceptualization; Junlin Wu: Data curation, validation; Chancui Deng: Visualization; Ning Gu: Methodology; Shuangya Yang: Investigation,; Guangtao Zhou: Formal analysis; Xiaoling Fu: Data curation, visualization; Ranzun Zhao: Investigation, Validation; Zhenglong Wang: Investigation, Data Curation; Yongchao Zhao: Data Curation, Formal Analysis; Bei Shi: Supervision—Review and Editing.

Funding

Declarations

Competing interests

The authors declare no competing interests.

Ethical approval

The ethical review methods were reviewed and approved by the Biomedical Research Ethics Committee of the Affiliated Hospital of Zunyi Medical University, including appropriate patient consent. We also strictly followed the protocol approved by the ethics committee to conduct the study and protect the health and rights of the subjects during the experimental process.

Additional information

Supplementary Information The online version contains supplementary material available at https://doi.org/10.1038/s41598-025-96991-8.

Correspondence and requests for materials should be addressed to R.Z., Z.W., Y.Z. or B.S.

Reprints and permissions information is available at www.nature.com/reprints.

Publisher's note Springer Nature remains neutral with regard to jurisdictional claims in published maps and institutional affiliations.